Proceedings of the 9th International Conference of Control, Dynamic Systems, and Robotics (CDSR'22)
Niagara Falls, Canada – June 02-04, 2022
Paper No. 180
DOI: 10.11159/cdsr22.180

Design of a Sensorless Field Oriented Control Drive for Brushless DC Motors

Shanthar Rajinth[1], Chamil Abeykoon[2], D. H. S. Maithripala[1]
[1]Department of Mechanical Engineering, University of Peradeniya
Peradeniya 20400, Sri Lanka
rajinthss@eng.pdn.ac.lk; smaithri@eng.pdn.ac.lk
[2]Department of Materials, Faculty of Science and Engineering, The University of Manchester
Oxford Road, M13 9PL, Manchester, UK
chamil.abeykoon@manchester.ac.uk

Abstract - Field Oriented Control (FOC) is a widely employed motor control methodology for Brushless DC (BLDC) motors. FOC requires an accurate measure of the rotor angular position for proper operation. Depending on how this rotor position is obtained, FOC can be implemented in either sensored mode or sensorless mode. Typically, sensored FOC employs position sensors to measure rotor angular position, whereas sensorless FOC estimates the rotor position using state observers based on currents, voltages and back electro motive forces (BEMF). This paper presents the first stage of a research aimed to identify an optimum observer type for a sensorless FOC, and it focuses in particular on the implementation of a Luenberger BEMF observer (LBO) based sensorless FOC system. Based on the mathematical formulation of the problem, the LBO was constructed to be a time-varying system, which introduced additional complexities when implementing the system in MATLAB. All simulations were carried out in the MATLAB Simulink environment according to predefined test criteria. The simulation results of the sensored FOC show accurate tracking of the reference speed and smooth transition dynamics, whereas the sensorless FOC simulations also indicate similar performance to the sensored case in general. However, a steady state speed ripple was noticed in the sensorless mode compared to sensored mode, along with increased settling times.

Keywords**:** Brushless DC (BLDC) Motor, Field Oriented Control (FOC), Luenberger BEMF Observer (LBO), Sensored Mode, Sensorless Mode

1. Introduction

BLDC motors have become increasingly common in various engineering applications such as robotics, electric vehicles, domestic appliances, power tools and Unmanned Aerial Vehicles (UAV). This is mainly due to the advantages offered by BLDC motors over Brushed DC (BDC) motors such as higher efficiency, higher operating speeds, high torque to weight ratio, reduced maintenance requirements and excellent dynamic response [1]. However, the control of a BLDC motor is a more complex task compared to their BDC counterparts, and the performance of the motor is directly dependent on the performance of the control algorithm. The most common method of driving a BLDC method is Trapezoidal control, which is also known as 6-Step commutation. Although this method is simple to implement, it has several drawbacks such as significant torque ripple, limited speed ranges and higher noise [2]. On the other hand, the FOC methodology overcomes these limitations while also delivering increased efficiency by maximizing the torque produced per unit current [3][4].

As mentioned, an accurate measure of the rotor angular position is mandatory for the FOC algorithm, and this can be obtained in two methods. The first method is to employ sensors such as Hall Effect sensors to determine the rotor position, known as sensored FOC [5]. This approach results in higher accuracy measurements, but in most cases undesirable due to cost, installation issues and limited application ranges [6]. The second method is to estimate the position using state observers, known as sensorless FOC. Here, the rotor position is estimated using measurable system parameters such as voltages and currents. This eliminates the requirement for physical sensors, thus reducing cost and increasing robustness albeit at lower accuracy levels [7]. Nevertheless, the advantages of sensorless FOC have made it a popular approach in the recent times [8]-[11].

Mariano and Scicluna [8] constructed and simulated a BEMF observer based sensorless FOC drive, where the speed error during steady state operation was zero. However, during transients the tracking of the observer has fluctuated (overshoot of 8%), but only temporarily before regaining the stability. This decreased transient performance has been attributed to the limitations of the controller bandwidth. In [9], Rau et al. have also developed a BEMF

observer based FOC system. However, their results display a high level of noise in rotor speed (approximately ±20 rpm). Colton [10] implemented a flux observer based sensorless controller and has highlighted the computational efficiency of this approach compared to other sensorless methods (such as BEMF based observers). Also, flux observers tend to perform better than BEMF observers at low rotor speeds (the exact limit depends on the motor and application, in this study it was found to be 450 rpm) due to rotor flux being independent of rotor speed, which is an added advantage [12]. A sensorless FOC drive based on a sliding mode observer has been simulated by Sandre-Hernandez et al [11], where the authors have compared the performance of conventional and modified sliding mode observer structures. The implementation of this kind of observer is simpler compared to that of other methods (such as BEMF and flux observers), and the results indicate good tracking and robustness of the algorithm.

Despite a substantial amount of literature being present on individual observer characteristics, a clear comparison between them using the same test conditions was not available. The scope of the present study is to bring these isolated findings to a common platform and addressing the knowledge gap, and the first step is successfully implementing and testing a Luenberger BEMF observer. Hence, the primary goal of this paper is to design, analyse and validate the performance of a sensorless FOC scheme employing a BEMF based Luenberger observer. Thereafter, the methodology adopted in this study would be used as a template to implement FOC with other types of observers, with the final aim of comparing all such observers under similar conditions. Such a comparison would be beneficial for anyone faced with the decision of selecting an observer for an application requiring sensorless FOC.

2. Sensored Field Oriented Control

2.1. Overview

The overall control system proposed in this study is depicted in Fig. 1. As seen, the position measure plays a crucial role in the algorithm, since it is required by the mathematical Park transformations. The system is cascaded, with a current control secondary inner loop and speed control primary outer loop. Sensorless FOC replaces the position sensor with a position observer. Moreover, the accurate rotor angular position is imperative for the proper functioning of the control system.

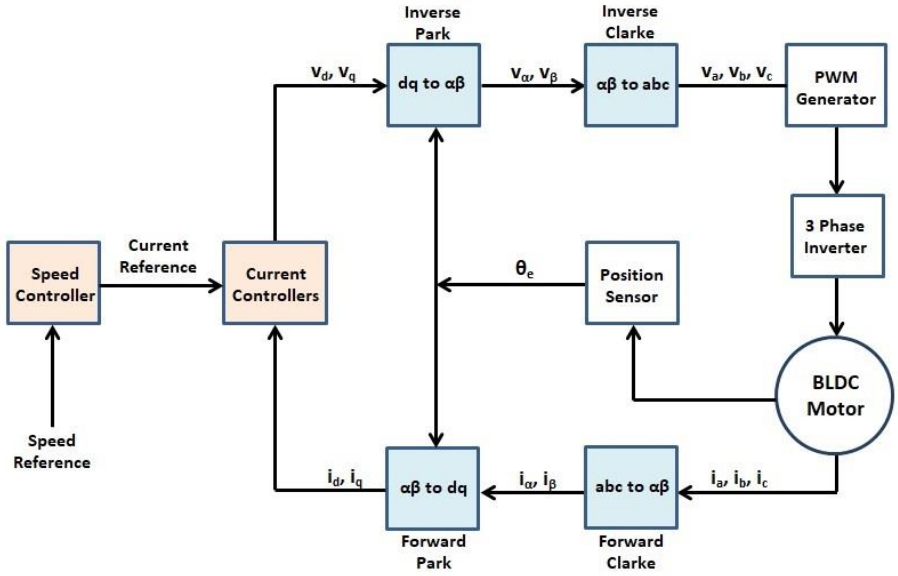

Fig. 1: Overall block diagram of FOC for this study.

The principle of the FOC algorithm is as follows. The three phase power supply to the motor generates a rotating stator magnetic field. The permanent magnets in the rotor attempt to align themselves along this field, resulting in a continuous rotation. The maximum torque is produced when the fields are perpendicular. The FOC algorithm achieves this condition by splitting the stator field into two perpendicular components, and then driving the component along the rotor field (non-torque producing) to zero. The axes along and perpendicular to the rotor field are termed the direct (*d*) and quadrature (*q*) axes, respectively.

2.2. Mathematical Model of the BLDC Motor

The mathematical model of the BLDC motor in the d-q reference frame can be expressed as given in Eqs. (1) - (4).

$$v_d = R_d i_d + L_d \frac{di_d}{dt} - \omega_e L_q i_q \tag{1}$$

$$v_q = R_q i_q + L_q \frac{di_q}{dt} - \omega_e (L_d i_d + \psi) \tag{2}$$

$$T_e = \frac{3}{2} P \psi i_q \tag{3}$$

$$T_e = \frac{J}{P} \frac{d\omega_e}{dt} + \frac{B}{P} \omega_e + T_l \tag{4}$$

where v, i, R, L, J, B and ψ denote voltage, current, resistance, inductance, rotor inertia, viscous damping coefficient and rotor magnetic flux, respectively. T_e and T_l denote the electromagnetic and load torques, respectively and ω_e denotes the electrical frequency of the rotor. P is the number of stator pole pairs. The subscripts d and q refer to the components along the d and q axes.

Note that in the model given above, Eqs. (1) - (3) are in the electrical domain, and the Eq. (4) is in the mechanical domain. Also it should be noted that the electromagnetic torque of the motor is proportional to the q axis current. This simplifies the cascaded control hierarchy since reference speed ω_e governs the required T_e, which can directly be converted into the required i_q using the above relationship in Eq. (3).

2.3. Current and Speed Controllers

The current and speed control loops are in a cascaded structure. Therefore, the individual performance as well as the inter-relationship between the controllers should be considered during the design stage. Generally, the inner loop should be much faster than the outer loop of a cascaded system for proper operation. This is to ensure that (a) when the output of the outer loop varies, it is quickly reflected by the inner loop (b) the inner loop is capable of regulating high frequency variations, which in this case are the currents. Therefore, the gains of the controllers are selected such that the inner current loop will be 20 times faster than the outer speed loop, which is the upper limit of the 10-20 range recommended in literature [8].

The system consists of PI controllers, which are more suitable than PID controllers. This is due to the sensitivity of the latter to noise and disturbances, which are inherent in electronic systems. The calculated PI controller gains are summarized in Table 1. Here, K_P is the proportional gain and K_I is the integral gain. A MATLAB script was written which contains the design parameters of the control system (i.e. time constants, damping ratio, bandwidth) and their relationships. The controller gains are automatically calculated upon execution of the script and fed into the Simulink model.

The block diagrams of the controllers are depicted in Fig. 2. The reference speed (ω^*) is specified by the user and is fed into the speed control system which outputs the quadrature current reference (i_q^*) in terms of the required electromagnetic torque (T_e). The direct current reference (i_d^*) is set to zero. These current references control the supply voltages to the BLDC motor. Furthermore, in Fig. 2a and Fig. 2b, the cross coupling terms of Eq. (1) and Eq. (2) are inverted and fed in as noise. This is done to decouple the current controllers, making the design procedure independent. In Fig.2c, the load torque is considered as an external disturbance. This simplifies the speed controller design.

Table 1: Calculated PI Controller Gains

Controller	Direct Current		Quadrature Current		Speed	
Gain	K_P	K_I	K_P	K_I	K_P	K_I
Value	0.05	626.9	0.05	626.9	0.0027	0.4807

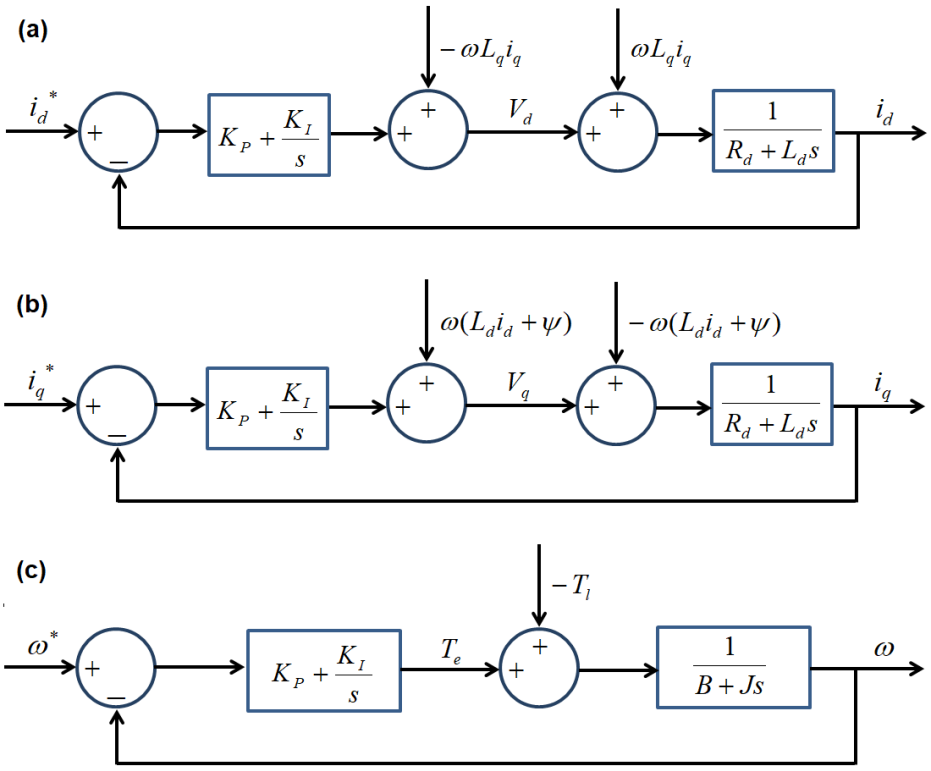

Fig. 2: (a) The direct current control diagram, where the reference is set to zero. (b) The quadrature current control diagram, where the reference is determined by the outer speed loop. (c) The rotor speed control diagram, where the reference is specified externally

3. Sensorless Field Oriented Control

As mentioned previously in Section 2.1, in the sensorless version of the FOC algorithm, the rotor position sensor is replaced by a rotor position observer. In this paper, a BEMF observer has been designed and simulated. For a linear system given by Eq. (5), a Luenberger observer can be formulated as given in Eq. (6) [3]. Here, A, B and C are the dynamic, input, and output matrices, respectively. The system states, inputs and outputs are denoted by x, u and y respectively. L is the Luenberger gain matrix, which governs the observer dynamics. $\hat{x}$ is the estimated state vector.

$$\dot{x} = Ax + Bu$$
$$y = Cx \tag{5}$$

$$\dot{\hat{x}} = (A - LC)\hat{x} + [B \quad L]\begin{bmatrix} u \\ y \end{bmatrix} \tag{6}$$

The state space formulation of the BEMF observer system is given in Eq. (7). The dynamic matrix depends on the rotor speed, resulting in a time-variant system [13]. Therefore, L should be varied accordingly. This is achieved by calculating and storing the L values for a given rotor speed range beforehand in a lookup table, and then reading the value corresponding to the current speed of the simulation. This approach reduces the computational burden of the simulation. For convenience, this formulation is done in the α-β frame, which results from the forward Clark transformation.

$$\begin{pmatrix} \dot{i_\alpha} \\ \dot{i_\beta} \\ \dot{e_\alpha} \\ \dot{e_\beta} \end{pmatrix} = \begin{bmatrix} -R/L & 0 & -1/L & 0 \\ 0 & -R/L & 0 & -1/L \\ 0 & 0 & 0 & -\omega_e \\ 0 & 0 & \omega_e & 0 \end{bmatrix} \begin{pmatrix} i_\alpha \\ i_\beta \\ e_\alpha \\ e_\beta \end{pmatrix} + \begin{bmatrix} 1/L & 0 \\ 0 & 1/L \\ 0 & 0 \\ 0 & 0 \end{bmatrix} \begin{pmatrix} v_\alpha \\ v_\beta \end{pmatrix} \tag{7}$$

$$\begin{pmatrix} i_\alpha \\ i_\beta \end{pmatrix} = \begin{bmatrix} 1 & 0 & 0 & 0 \\ 0 & 1 & 0 & 0 \end{bmatrix} \begin{pmatrix} i_\alpha \\ i_\beta \\ e_\alpha \\ e_\beta \end{pmatrix}$$

Here, *i*, *v* and *e* refer to the supply currents, supply voltages and BEMF voltages, respectively. The subscripts α, β denote the components along those axes. Using this representation, the corresponding Luenberger observer can be formulated according to Eq. (6). The state vector will contain the estimated BEMF values which can be used to calculate the rotor angular position θ_e as given by Eq. (8).

$$\theta_e = -tan^{-1}\left(\widehat{e_\alpha}/\widehat{e_\beta}\right) \tag{8}$$

For proper operation, the observer of a system should be sufficiently faster than the system itself. Therefore, in this case, the *L* gain matrix, which governs observer dynamics, is specified such that the observer will be 8 times faster than the system (the theoretically recommended range is 5-10 times). Eq. (8) shows that the observer can divide the estimated BEMF waveforms to obtain the rotor position. However, this approach results in significant noise and reduced accuracy. Therefore, the rotor position is typically obtained using a Phase Locked Loop (PLL) subsystem [8]. The gains used for the current controllers (presented in Table 1) were found out to work well for the PLL controller as well, therefore the same values have been used.

4. Modeling and Simulation

4.1. General Information

The system was implemented and simulated using MATLAB Simulink with a fixed step time of 1 µs. Trials revealed that although smaller time steps increased the simulation runtime, the accuracy improvement of the results were negligible. The overall model is shown in Fig. 3. The details of the main subsystems are as follows.

- BLDC Motor: Contains the BLDC motor model, and the motor parameters used for the simulation are given in Table 2.
- Control Block: Contains the speed and current controllers in a cascaded format.
- SVPWM Generator: Contains a 2-Level Space Vector Pulse Width Modulation (SVPWM) generator which produces the gate pulses for the inverter.
- 3 Phase Inverter: Contains a 3 leg MOSFET based inverter which converts DC signals to AC signals.
- Observer: Contains the LBO model.
- Load Torque: This block is used to input the virtual torque attached to the motor shaft.
- Reference Speed: This block is used to specify the speed reference for the motor.

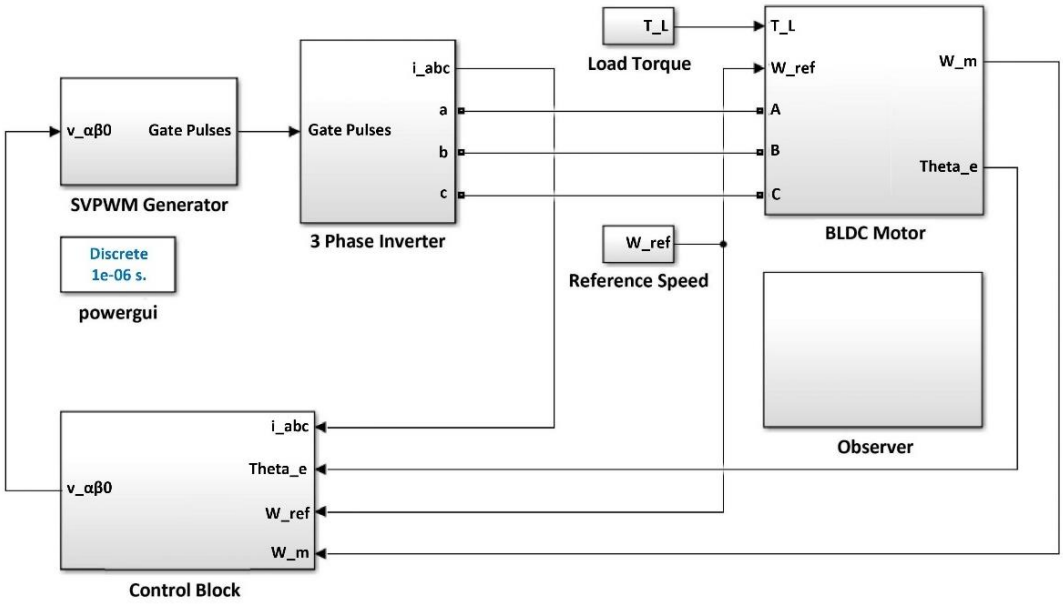

Fig. 3: The overall MATLAB Simulink model of the control system (The main components shown as blocks contain several subsystems within them).

Table 2: Physical Parameters of the BLDC Motor Model

Parameter	Value	Unit
Stator Resistance ($R_{d,\,q}$)	0.1223	Ω
Stator Inductance ($L_{d,\,q}$)	9.75 x 10^{-6}	H
Rated Voltage (V_{DC})	11	V
No. of Pole Pairs (P)	7	-
Full Load Torque(T)	0.1432	Nm
Rotor Flux Linkage (ψ)	0.0012	Wb
Rotor Inertia (J)	7.312 x 10^{-6}	kgm^{-2}
Viscous Damping Coefficient (B)	7.312 x 10^{-7}	Nms

4.2. Simulation Criteria

BEMF based observers are not capable of operating at low speeds (below 450 rpm in this case), due to the BEMF magnitudes being too small and error prone. Therefore, when using such observers the usual approach is to start the algorithm in open loop mode. After acquiring sufficient speed and BEMF magnitudes, the algorithm then switches to closed loop sensorless mode. With regard to this, the term switching will refer to this phenomenon henceforth.

- At 0.00 seconds: Open loop mode
- At 0.00 seconds: Reference speed set to 3000 rpm
- At 0.00 seconds: Full load torque of 0.1432 Nm applied
- At 0.10 seconds: Switching
- At 0.25 seconds: Reference speed decreased to 1500 rpm

This ensures a well-rounded performance characteristic which includes transient dynamics, steady state operation and speed tracking.

5. Simulation Results and Discussion

5.1. Sensored Field Oriented Control Simulation

The observed variation of speed of the sensored control algorithm is shown in Fig. 4a. As can be seen from Fig. 4a, the algorithm shows excellent tracking with an overshoot of less than 2% and a settling time of less than 0.05 seconds. The transition dynamics are smooth as well. Fig. 4b shows the rotor position variation with time. When the speed is changed from 3000 rpm to 1500 rpm, the frequency of the wave has halved as expected. The major task of the sensorless algorithm is to reconstruct this waveform.

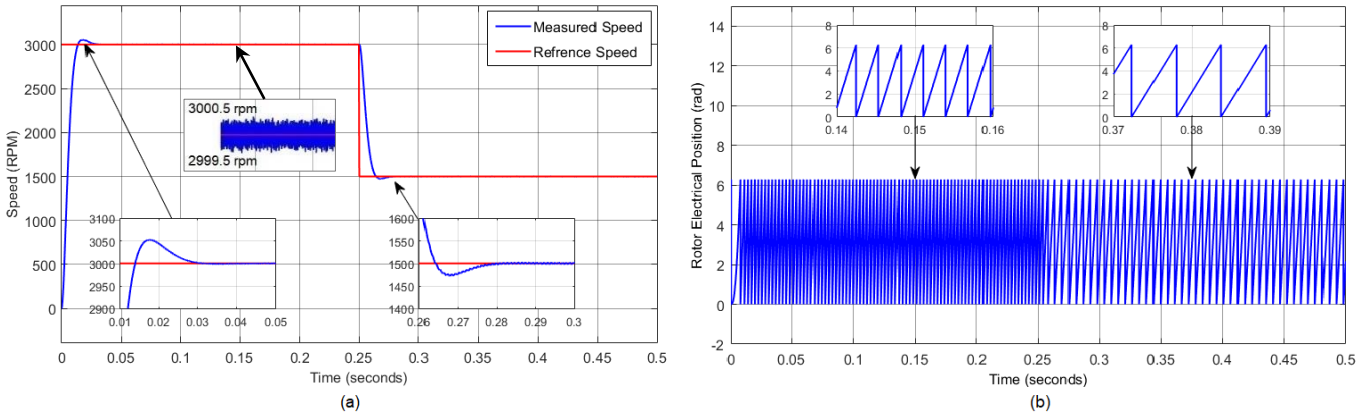

Fig. 4: (a) Variation of speed with time in sensored mode. (b) Variation of rotor angular position with time.

5.2. Sensorless Field Oriented Control Simulation

The speed tracking simulation results of the LBO are given in Fig. 5a. When the switching occurs, the speed drops to around 2400 rpm, before quickly regulating itself. The speed settles at 3000 rpm in approximately 0.03 seconds, but a steady state ripple of ±15 rpm can be observed at 3000 rpm. After reference speed is reduced to 1500 rpm, the speed ripple reduces to ±10 rpm. The variation of the actual and estimated rotor position is given in Fig. 5b. When the switching occurs, the estimated position momentarily drops but manages to successfully track the actual position. However, an error in the form of a lag of approximately 0.17 rad at 3000 rpm and 0.16 rad at 1500 rpm can be observed. This is most likely caused by practical limitations of the observer.

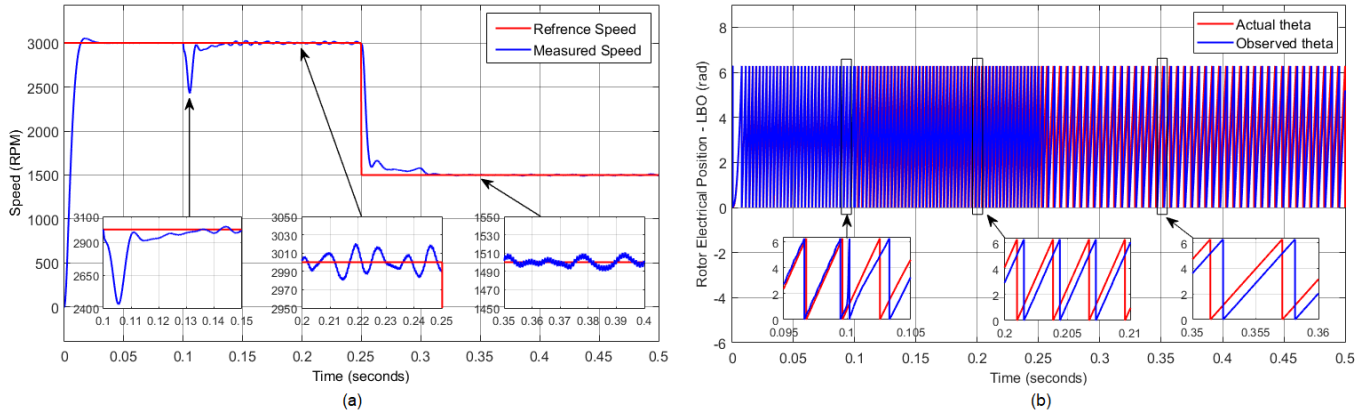

Fig. 5: (a) Variation of speed with time in sensorless mode (b) Variation of rotor angular position with time

A summary of the key performance characteristics of the sensorless FOC scheme is given in Table 3.

Table 3: Summary of sensorless FOC performance characteristics

Parameter	Value
Switching speed drop	600 rpm
Settling time after switching	0.03 s
Steady state speed ripple (3000 rpm)	±15 rpm
Steady state speed ripple (1500 rpm)	±10 rpm
Steady state position error (3000 rpm)	0.17 rad
Steady state position error (1500 rpm)	0.16 rad

5.3 Sensored Field Oriented Control Discussion

The results obtained for the sensored FOC algorithm which were presented in Section 5.1 are in accordance with the standard results present in the literature [8][14]. The speed variation shown in Fig. 4 shows that the system tracks the reference speed extremely well. The overshoot is minimal, which complies with the damping ratio of 0.707 specified during the design stages. The settling time is less than 0.05 and transient dynamics are also smooth. Upon close inspection of the speed variation plot, a low magnitude high frequency noise component can be identified (Fig. 4a). This is most likely caused by the high frequency switching of the 3 phase voltage inverter, which produces voltage spikes during each switching event.

5.4 Sensorless Field Oriented Control Discussion

The speed tracking of the LBO as shown in Fig. 5a indicates satisfactory performance of the control algorithm. Although there is a sharp drop in speed during switching, the motor speed has returned to the reference value in a short time duration (within 0.05 seconds). However, a ripple in the speed is observed, which is present in varying magnitudes throughout the simulation. During iterative simulations, it was found out that the magnitudes of the ripples correlated to the PI gain values. These ripples could be reduced to under ±15 rpm by adjusting the gains, but completely eliminating them was not possible.

The position tracking of the LBO is shown in Fig. 5b, and a lagging error was visible between the estimated and actual rotor positions. This error is most likely to be caused by the bandwidth limits of the observer. Although increasing the observer bandwidth can reduce the error, it leads to extremely large gains and unrealistic control inputs. Overall, throughout the simulation the errors in speed tracking were maintained under 0.7% of the reference values, and the position errors were constrained to under 9^{o} degrees.

6. Conclusions

The main aim of this study was to simulate and evaluate the performance of a sensored FOC and sensorless FOC algorithm using a Luenberger BEMF observer. The methods used and the results obtained will be later extended to analysing other observer types, with the aim of comparing and determining the most optimal observer type. The results obtained show accurate tracking of the reference speed and smooth transition dynamics of the sensored FOC algorithm, supporting its widespread use in high end applications such as industrial robotics, UAVs and electric vehicles. Satisfactory results were obtained from the sensorless FOC scheme as well, which employed a Luenberger BEMF observer. Although performance fluctuations were noticed at certain instances of the simulation, the overall performance of the model demonstrates the capability of reliable operation of FOC without the presence of a physical position sensor. The errors in speed and position were maintained within narrow margins as mentioned in Section 5.4. Thus, the performance of the LBO is validated, and can be considered as that of a typical Luenberger observer in future comparisons.

References

[1] A.A Mousmi and Y. El Houm, “Trapezoidal control of Brushless DC motor based on DSP F28335”, *International Conference on Wireless Technologies, Embedded and Intelligent Systems (WITS),* 2017, pp. 1-5

[2] F. Golesorkhie, F. Yang, L. Vlacic, G. Tansley, “Field Oriented Control-Based Reduction of the Vibration and Power Consumption of a Blood Pump”, *Energies.* 2020; 13(15):3907

[3] J. R. Mevey, “Sensorless Field Oriented Control of Brushless Permanent Magnet Synchronous Motors”, MSc dissertation, Department of Electrical and Computer Engineering, College of Engineering, Kansas State University, Manhattan, Kansas.

[4] L. Chunhua and Y. Luo, “Overview of advanced control strategies for electric machines”, *Chinese Journal of Electrical Engineering.* 3. 2017, 53-61

[5] N. Biniakos, V. Iakovakis, “Sensored Field Oriented Control of BLDC Motor for Pico Satellite Attitude Control”, *International Journal of Innovative Science and Research Technology*. 4, 2019

[6] J.C. Gamazo-Real, E. Vázquez-Sánchez, J. Gómez-Gil, “Position and Speed Control of Brushless DC Motors Using Sensorless Techniques and Application Trends”, *Sensors.* 2010; 10(7):6901-6947

[7] P.P. Acarnley and J.F. Watson, “Review of position-sensorless operation of brushless permanent-magnet machines”, in *IEEE Transactions on Industrial Electronics*, vol. 53, no. 2, pp. 352-362, April 2006

[8] M. Mariano and K. Scicluna, “Design and Implementation of an Electronic Speed Controller for Brushless DC motors”, 2017

[9] D. Rau, J. Rodina, P. Hubinsky, “Sensorless field oriented control of BLDC motors for MAVS”, *Transactions on Electrical Engineering,* 2015

[10] S. Colton, “Flux Observer-Based Sensorless Field-Oriented Control of Surface Permanent Magnet Synchronous Motor”, (Gen. 1). 3 Feb. 2014

[11] O. Sandre-Hernandez, P. Ordaz-Oliver and C. Cuvas-Castillo, “Sensorless Field Oriented Control of BLDC motor based on Sliding Mode Observer”, 2*019 International Conference on Mechatronics, Electronics and Automotive Engineering (ICMEAE),* 2019, pp. 119-124

[12] W. D. Drury, D. Holliday and P. H. Mellor, “A Comparison of a Flux Observer with a Back-Emf Technique for Sensorless Rotor Position Estimation”, *Proceedings of the 41st International Universities Power Engineering Conference,* 2006, pp. 714-718

[13] O. Orozco, C. Castaneda, A. Rodríguez-Herrero, G. García-Sáez, E. Hernando, “Linear Time-Varying Luenberger Observer Applied to Diabetes”, *IEEE Access*, 2018.

[14] J. P. John, S. S. Kumar, B. Jayam “Space Vector Modulation based Field Oriented Control Scheme for Brushless DC Motors”, *Proceedings of ICETECT,* 2011